Can optimized model-based iterative reconstruction improve the contrast of liver lesions in CT?

Acta Radiologica
2023, Vol. 64(1) 42–50

DOI: 10.1177/02841851211070119
journals.sagepub.com/home/acr

Jonas Oppenheimer[1], Keno Kyrill Bressem[1,2], Fabian Henry Jürgen Elsholtz[1], Bernd Hamm[1] and Stefan Markus Niehues[1]

Abstract

Background: Computed tomography is a standard imaging procedure for the detection of liver lesions, such as metastases, which can often be small and poorly contrasted, and therefore hard to detect. Advances in image reconstruction have shown promise in reducing image noise and improving low-contrast detectability.

Purpose: To examine a novel, specialized, model-based iterative reconstruction (MBIR) technique for improved low-contrast liver lesion detection.

Material and Methods: Patient images with reported poorly contrasted focal liver lesions were retrospectively reconstructed with the low-contrast attenuating algorithm (FIRST-LCD) from primary raw data. Liver-to-lesion contrast, signal-to-noise, and contrast-to-noise ratios for background and liver noise for each lesion were compared for all three FIRST-LCD presets with the established hybrid iterative reconstruction method (AIDR-3D). An additional visual conspicuity score was given by two experienced radiologists for each lesion.

Results: A total of 82 lesions in 57 examinations were included in the analysis. All three FIRST-LCD algorithms provided statistically significant increases in liver-to-lesion contrast, with $FIRST_{MILD}$ showing the largest increase (40.47 HU in AIDR-3D; 45.84 HU in $FIRST_{MILD}$; $P < 0.001$). Substantial improvement was shown in contrast-to-noise metrics. Visual analysis of the lesions shows decreased lesion visibility with all FIRST methods in comparison to AIDR-3D, with $FIRST_{STR}$ showing the closest results ($P < 0.001$).

Conclusion: Objective image metrics show promise for MBIR methods in improving the detectability of low-contrast liver lesions; however, subjective image quality may be perceived as inferior. Further improvements are necessary to enhance image quality and lesion detection.

Keywords
Model-based iterative reconstruction, hybrid iterative reconstruction, computed tomography, liver, liver lesion, low-contrast detectability

Date received: 2 May 2021; accepted: 13 December 2021

Introduction

Computed tomography (CT) imaging of the liver represents a routine diagnostic tool for staging examinations and to evaluate disease progression for most malignant diseases. The liver represents the most common site of distant metastases (1,2). The sensitivity of CT for the detection of metastases has been reported from 64.7%–83.6%, with magnetic resonance imaging (MRI) and positron emission tomography (PET) showing better sensitivity and specificity (3–5). Small lesions, with diameters <10 mm, have a very poor detection rate in CT (6). Small, indeterminate lesions

[1]Department of Radiology, Charité, Universitätsmedizin Berlin, corporate member of Freie Universität Berlin and Humboldt-Universität zu Berlin, Berlin, Germany
[2]Berlin Institute of Health at Charité, Universitätsmedizin Berlin, Berlin, Germany

Corresponding author:
Jonas Oppenheimer, Charité – Universitätsmedizin Berlin, Clinic for Radiology Campus Benjamin Franklin, Hindenburgdamm 30, 12203 Berlin, Germany.
Email: jonas.oppenheimer@charite.de

have been reported in up to one-third of CT examinations. The difficulty of determining the origin and relevance of such small lesions has also been discussed, with up to one-quarter of these lesions being potentially malignant (7–10).

Advances in image reconstruction techniques have been used to reduce image noise in CT images and improve the detectability of low-contrast lesions. Hybrid iterative reconstruction (HIR) algorithms have mostly replaced filtered back projection (FPB) reconstructions, as they show a potential for dose reductions up to 50% with maintained or even decreased image noise (11–14). By now, all major vendors offer HIR algorithms, with some variations of the basic technique of image reconstruction (15).

Further improvements on these algorithms, combined with advances in computing capacities, have given way to pure or model-based iterative reconstructions (MBIR). These methods do not use back projections as a basis for the image, but instead start with a forward projection of the image, based on statistical models of image noise, scanner and detector characteristics, and properties of the X-ray beams (16,17). Some promising results have been shown in the comparison of MBIR with HIR and FBP, with further noise reduction and image improvement (18–20).

Some vendors have begun offering MBIR with presets for certain organ systems or tasks. One such option is the Forward Projected Iterative Reconstruction SoluTion (FIRST; Canon Medical Systems Corporation, Otawara, Japan), which offers a "Low-Contrast-Detectability Brain" setting, aiding in the detection of poorly contrasted brain lesions. This application has shown the ability to reduce the necessary radiation dose by 50%, while maintaining detectability in a brain phantom (21,22). The aim of the present study was to test the transfer of the FIRST algorithm on to poorly contrasted focal liver lesions and to compare it with the currently used HIR method.

Material and Methods

Patients

The need for an ethics vote was obtained for this retrospective study by our institutional review board (EA4/140/17).

All abdominal CT studies performed between 22 January 2019 and 27 February 2020 on a suitable CT device were reviewed in our institution's reporting system (Centricity 6.0; GE Healthcare, Barrington, IL, USA).

Further inclusion criteria were examinations with one or more reported poorly contrasted low attenuation focal liver lesions (FLL) (Fig. 1) and studies with at least a venous contrast phase (80-s delay).

Exclusion criteria were as follows: examinations with more than five poorly contrasted lesions; examinations with more than five lesions classified as malignant additionally to any poorly contrasted FLL; poorly contrasted areas of the liver, not described as focal; hyperdense lesions; and patients with a primary liver disease, such as hepatocellular carcinoma or known cystic disease.

Sex, age at examination, imaging indication, and radiation dose as dose-length product were noted for each patient. It was recorded if further benign or malignant lesions were seen in the liver and if the primary radiologist classified the lesion as benign, malignant, or unclassifiable. Each lesion was treated as its individual entity if multiple lesions were present in a single exam.

CT protocol

All CT studies were performed on a Canon Aquilion ONE Genesis Edition (Canon Medical System Corp., Otawara, Japan), a 320-row CT device with a minimal z-axis resolution of 0.5 mm and width of 16 cm. It utilizes an automatic dose exposure system ("Patient Adaptive Exposure"). It offers

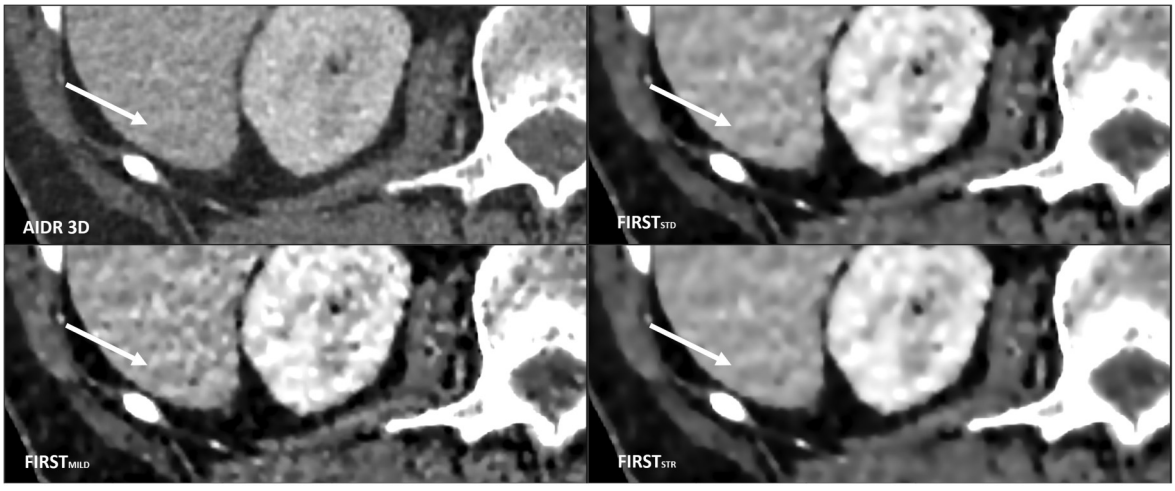

Fig. 1. Axial computed tomography of the abdomen in venous phase, exemplary poorly contrasted focal liver lesion in all reconstruction methods (arrows).

image reconstruction with FBP, HIR, and MBIR. An abdominal scan was obtained for each patient with an automatic patient-adapted voltage and amperage in the range of 100–120 kV and 100–700 mA. Image noise was set to 10. Exam pitch was 0.813 with a rotation time of 0.5 s. Collimation was set to 80 × 0.5 mm. Weight-adapted contrast medium (80–120 mL of Imeron® 400 MCT [Bracco Imaging Deutschland GmbH, Konstanz, Germany], Ultravist® 370 [Bayer AG, Leverkusen, Germany], or Xentix® 350 [Guerbet, Villepinte, France]) was applied to the patient. A venous contrast phase was acquired at 80 s of delay.

Initial image reconstruction was performed with the manufacturer's HIR algorithm, Adaptive Iterative Dose Reduction 3D (AIDR-3D; Canon Medical Systems Corporation, Otawara, Japan), which was FDA approved in 2012 (23). This method is routinely used at our institution. The standard setting for abdominal reconstruction at our institution is the "eSTD venose Phase Body FC18-H" kernel. Image reconstruction was performed with a slice thickness of 1.0 mm. This algorithm uses models of statistical noise and scanner features to implement a noise reduction in the projection data. A back projection is combined with the noise reduction to maintain image features (24).

The AIDR-3D Algorithm was compared with the proprietary MBIR algorithm, Forward Projected Model-Based Iterative Reconstruction SoluTion (FIRST) Low Contrast Detectability (LCD) (FIRST-LCD; Canon Medical Systems Corporation, Otawara, Japan). This algorithm offers three settings, standard ($FIRST_{STD}$), mild ($FIRST_{MILD}$), and strong ($FIRST_{STR}$). It was FDA approved in November 2016 (25). This algorithm performs a forward projection in each iteration, using a statistical model to develop an initial image. Noise features such as photon starvation, anatomical noise, quantum noise, and electrical noise are included in the model, as well as characteristics of the scanner device itself and the radiation beam. A fully synthetic image is then iteratively compared to the measured values for data consistency until an optimal image is reconstructed (26). The primary data for each study were reconstructed with all three FIRST settings.

Evaluation of contrast, signal-to-noise ratio, and contrast-to-noise ratio

Objective evaluation of the lesions was performed on Visage 7.1 (PRO Medicus Ltd., Richmond, VIC, Australia). For each lesion, the axial slice in which it presented as largest in the AIDR-3D reconstruction was selected. A freehand region of interest (ROI) was drawn at the lesion's borders, excluding surrounding healthy liver tissue. Three circular ROIs with a diameter of 10.0 mm were placed in direct proximity of the lesion into healthy parenchyma. Each ROI was placed at least 1.0 mm away from the lesion ROI to exclude an overlap in attenuation values. The ROIs were also placed outside of large vessels. The average attenuation of the lesion ROI was defined as the lesion attenuation. The standard deviation (SD, σ) of the attenuation values was defined as lesion noise. The signal-to-noise-ratio (SNR) was defined as the ratio of lesion attenuation to lesion noise. The combined average attenuation of all three liver ROIs was calculated as the liver attenuation and the combined average SD as liver noise. The difference between the liver attenuation and lesion attenuation was defined as the liver-to-lesion-contrast (LLC). A further ROI with a diameter of 50.0 mm was placed centrally into the imaged air above the patient. The SD of the attenuation values of this ROI was used as a measure for background noise. A contrast-to-liver- noise-ratio (CNR_L) was defined as proportion of LLC to liver noise. A contrast-to-background-noise-ratio (CNR_{BG}) was defined as the ratio of LLC to the SD of the air ROI (Table 1). The ROIs were transferred into the exact position in each FIRST reconstruction using a copy and paste method provided by the software (Fig. 2).

Evaluation of subjective lesion impression

Subjective evaluation was performed with Centricity RA1000 Radiology Workstation 4.0 (GE Healthcare, Barrington, IL, USA). Two radiologists with 19 and 4 years of experience, respectively, in abdominal CT diagnostics were shown each lesion in all reconstructions. A single slice at fixed zoom was shown for each in a 2 × 2 grid, with a random order of images. Readers were blinded to the used algorithm. The standard presets for abdominal evaluation used at our institution were implemented, with a window level of 50 Hounsfield Units (HU) and width of 400 HU. If multiple lesions were visible in the image, an arrow in the top left image showed the lesion to be evaluated. Each reader rated each lesion in each reconstruction on a Likert-scale of 1 to 4, to avoid a mean value (1 point = clearly visible lesion, 2 points = well visible lesion, 3 points = poorly visible lesion, and 4 points = non-discernable lesion).

Table 1. Calculation of objective lesion parameters.

LLC	$= \textit{average attenuation liver ROIs} - \textit{average attenuation lesion ROI}$
SNR	$= \frac{\textit{average attenuation lesion ROI}}{\sigma\ \textit{lesion ROI}}$
CNR_L	$= \frac{LLC}{\sigma\ \textit{liver ROIs}}$
CNR_{BG}	$= \frac{LLC}{\sigma\ \textit{background ROI}}$

σ, standard deviation; CNR_{BG}, contrast-to-noise ratio with background noise; CNR_L, contrast-to-noise ratio with image noise in liver; LLC, liver-to-lesion contrast; ROI, region of interest; SNR, signal-to-noise ratio.

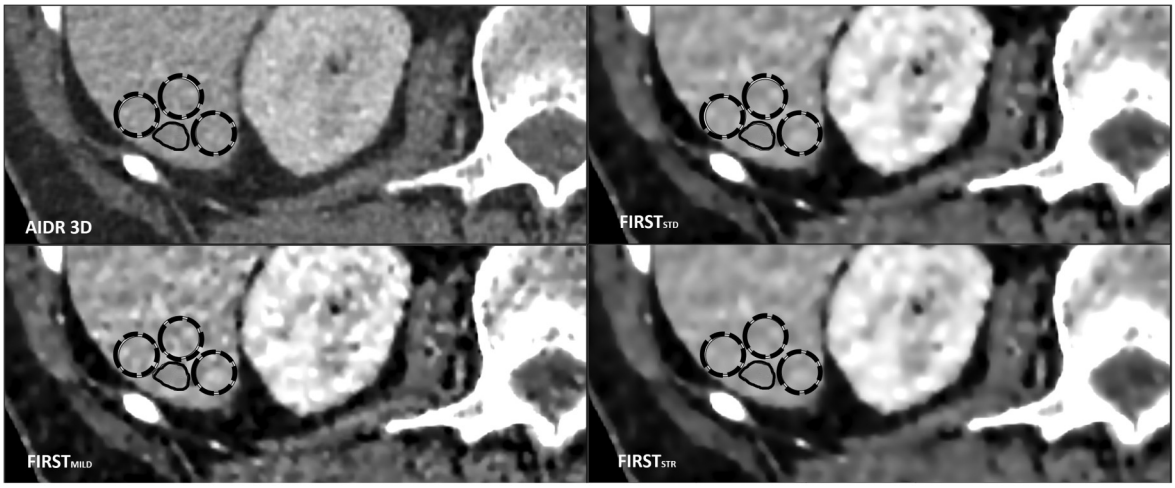

Fig. 2. Exemplary placement of the ROI measurements in axial computed tomography images: liver ROIs (thin, continuous line) and lesion ROI (thick, dashed line) for liver-to-lesion contrast calculation. ROI, region of interest.

Table 2. Patient and lesion characteristics.

Female-to-male ratio	20:37 (35.1%/64.9%)
Age at examination (years)	65.67 ± 10.70 (36–83)
Lesions per case	
1	43 (75.4)
2	6 (10.5)
3	6 (10.5)
4	1 (1.8)
5	1 (1.8)
Likely malignant lesions	
Likely	37 (45.1)
Possibly	2 (2.4)
Non-classifiable	15 (18.3)
Likely benign lesions (n = 28, 34.1%)	
Focal fatty tissue	12 (14.6)
Hemangioma	12 (14.6)
Unclear differential	9 (11)
Abscess	5 (6.1)
Cyst	4 (4.9)
Perfusion artefact	2 (2.4)
Diaphragm movement	1 (1.2)

Values are given as n (%) or mean ± SD (range).

Statistical analysis

Statistical analysis was performed with SPSS Statistics version 25 (IBM Corp., Armonk, NY, USA). Parametric data are presented as mean values and the SD of the mean. Non-parametric data are presented with the mean and median value as well as quartiles. Subjective viewer ratings, as ordinal data, were defined as non-parametric. The LLC, SNR, CNR_L, CNR_{BG}, and combined visual scores were compared among all four reconstruction methods. For parametric data, a repeated measures ANOVA test was used to compare the four groups. If the Mauchly test showed a significant result of <0.05, a Greenhouse–Geisser correction was employed when Epsilon was <0.75; in other cases, a Huynh–Feldt correction was used. A Friedman test with paired comparisons was used for comparison of non-parametric data. A subgroup analysis was performed for very small lesions, with an area <78.5 mm^2 (corresponding to a diameter of 10.0 mm in a round lesion) and for very low-contrast lesions. Very low-contrast lesions were defined as lesions with an LLC in the original reconstruction below the difference of the average LLC of all lesions and 1 SD of this average. A total of 15 statistical tests were performed, five each for the entire dataset and the two subgroups. A Bonferroni correction was applied to all *P* values. A corrected *P* value <0.05 was defined as a statistically significant difference between the four groups.

Results

Patient population and dose

From 2475 abdominal CT scans assessed, a total of 91 exams had reported poorly contrasted liver lesions; 34 scans met the exclusion criteria due to disseminated poorly contrasted lesions (19), disseminated other malignant lesions (5), both (3), or lack of primary imaging in the comparative reconstruction method (7). A total of 57 scans were included in the study. Patient and lesion characteristics are given in Table 2. Average dose-length product of the exams was 501.64 mGy*cm (range = 127.2–3438.2 mGy*cm; median = 353.0 mGy*cm).

Lesions

A total of 82 lesions were included in the 57 examinations (average = 1.44 lesions per exam). The average area of the

Table 3. Overview of objective results.

	AIDR-3D	$FIRST_{STD}$	$FIRST_{MILD}$	$FIRST_{STR}$
Lesion attenuation	82.73 ± 26.60 (8.7–186.2)	82.08 ± 28.36 (3.1–186.4)	79.46 ± 29.25 (–6.3 to 186.4)	82.71 ± 28.09 (5.6–186.1)
Liver attenuation	123.20 ± 27.43 (72.73–224.20)	125.02 ± 32.29 (68.47–224.20)	125.30 ± 32.50 (68.83–224.63)	125.45 ± 32.03 (68.03–224.20)
Lesion signal (HU)	40.47 ± 18.70 (6.33–113.87)	42.94 ± 21.03 (0.37–130.17)	45.84 ± 22.61 (1.63–136.20)	41.74 ± 20.48 (–0.17 to 127.97)
SNR*	3.61 3.47 (0.18–11.14); 2.57–4.42	4.37 3.96 (0.20–13.66); 2.72–5.51	3.34 3.15 (–0.29 to 8.07); 2.20–4.25	4.70 4.15 (0.31–14.03); 2.91–6.13
CNR_L*	2.11 2.00 (0.19–5.84); 1.53–2.60	3.24 3.03 (0.02–13.66); 2.78–4.10	2.34 2.25 (0.04–8.55); 1.52–3.00	3.61 3.34 (–0.01 to 11.71); 2.59–4.55
CNR_{BG}*	1.28 1.27 (0.04–4.13); 0.64–1.74	8.87 3.53 (0.001–54.49); 1.74–12.32	9.55 3.68 (0.004–62.39); 1.73–13.22	8.73 3.39 (–0.0004 to 53.69); 1.68–12.18

Values are given as mean ± SD
(range) unless otherwise indicated.
*Values are given as median
(range); 25P–75P.
25P, 25th percentile; 75P, 75th percentile; CNR_{BG}, contrast-to-noise ratio with background noise; CNR_L, contrast-to-noise ratio with image noise in liver; SNR, signal-to-noise ratio.

Table 4. Visual lesion evaluation.

	AIDR-3D	$FIRST_{STD}$	$FIRST_{MILD}$	$FIRST_{STR}$
Viewer 1	2.14 (2.0; 1.0–3.0)	2.22 (2.0; 2.0–3.0)	2.39 (2.0; 2.0–3.0)	2.12 (2.0; 1.0–3.0)
Viewer 2	2.54 (3.0; 2.0–3.0)	2.77 (3.0; 2.0–3.0)	2.79 (3.0; 2.0–3.0)	2.79 (3.0; 2.0–3.0)
Average ($P < 0.001$)	2.34 (2.5; 1.5–3.0)	2.49 (2.5; 2.0–3.0)	2.59 (2.5; 2.0–3.0)	2.46 (2.5; 2.0–3.0)

Values in parentheses are median; 25P–75P.
25P, 25th percentile; 75P, 75th percentile.

lesions was 1.45 cm^2 (range = 0.1–6.3 cm^2; median = 1.1 cm^2). In total, 37 lesions were noted as likely to be malignant by the primary radiologist and 28 were defined as likely benign. Other, non-poorly contrasted seemingly malignant lesions were noted on 3 (5.3%) scans. Other benign lesions were noted on 21 (36.8%) scans, with cysts noted in all cases and additional hemangiomas in 3 (14.3%) cases.

Signal, CNR, SNR, and SNR-liver

In the original AIDR-3D reconstruction, the average lesion contrast was 40.47 HU. While the average lesion contrast increased with all three FIRST settings, the SD of the average lesion contrast also increased. The difference in lesion contrast among the four reconstructions was statistically significant ($P < 0.001$). Lesion SNR was highest with $FIRST_{STR}$ at 4.70 followed by $FIRST_{STD}$. $FIRST_{MILD}$ showed an inferior SNR of 3.34 compared to 3.61 in the original AIDR-3D setting ($P < 0.001$), with $FIRST_{MILD}$ displaying a lower average lesion attenuation in comparison to AIDR-3D. However, in the evaluation of CNR_{BG}, $FIRST_{MILD}$ showed the highest value of all reconstructions at 9.55, with all FIRST reconstructions having a significantly larger CNR_{BG} than AIDR-3D ($P < 0.001$). In CNR_L evaluation, $FIRST_{STR}$ (3.61) and $FIRST_{STD}$ (3.24) were superior to $FIRST_{MILD}$ (2.34) and AIDR (2.11; $P < 0.001$). Detailed results are displayed in Table 3.

Subjective visual analysis

Average combined viewer rating for AIDR-3D lesions was 2.34. Visual rating was significantly inferior in all three FIRST reconstructions. $FIRST_{STR}$ scored best of the FIRST reconstructions. Full viewer ratings are given in Table 4. Viewer 1 found a minimal superiority of $FIRST_{STR}$ images in comparison to AIDR-3D.

Evaluation of small lesions

A total of 31 lesions had an area below the threshold of 78.5 mm^2. The average lesion signal showed a marked increase in contrast with $FIRST_{MILD}$ to AIDR-3D of 8.89 HU. Signal increase with $FIRST_{STD}$ and $FIRST_{STR}$ was moderate. Increases in CNR_{BG} and CNR_L with all three FIRST settings were statistically significant. SNR calculation showed a significant decrease with $FIRST_{MILD}$, with both other settings increasing this metric. Visual analysis

Table 5. Evaluation of small lesions.

	AIDR-3D	$FIRST_{STD}$	$FIRST_{MILD}$	$FIRST_{STR}$
Signal (HU) ($P < 0.001$)	49.17 (45.40)	52.84 (49.93)	58.06 (55.63)	50.96 (47.73)
SNR ($P < 0.001$)	3.65 (3.39)	4.27 (3.58)	3.14 (2.86)	4.59 (3.71)
CNR_L ($P < 0.001$)	2.61 (2.53)	3.97 (3.57)	3.00 (2.71)	4.34 (3.83)
CNR_{BG} ($P < 0.001$)	1.57 (1.43)	11.08 (4.31)	12.30 (4.71)	10.84 (4.39)
Viewer rating ($P = 1.0$)	2.26 (2.0)	2.35 (2.5)	2.44 (2.5)	2.34 (2.5)

Values in parentheses are median.
CNR_{BG}, contrast-to-noise ratio with background noise; CNR_L, contrast-to-noise ratio with image noise in liver; SNR, signal-to-noise ratio.

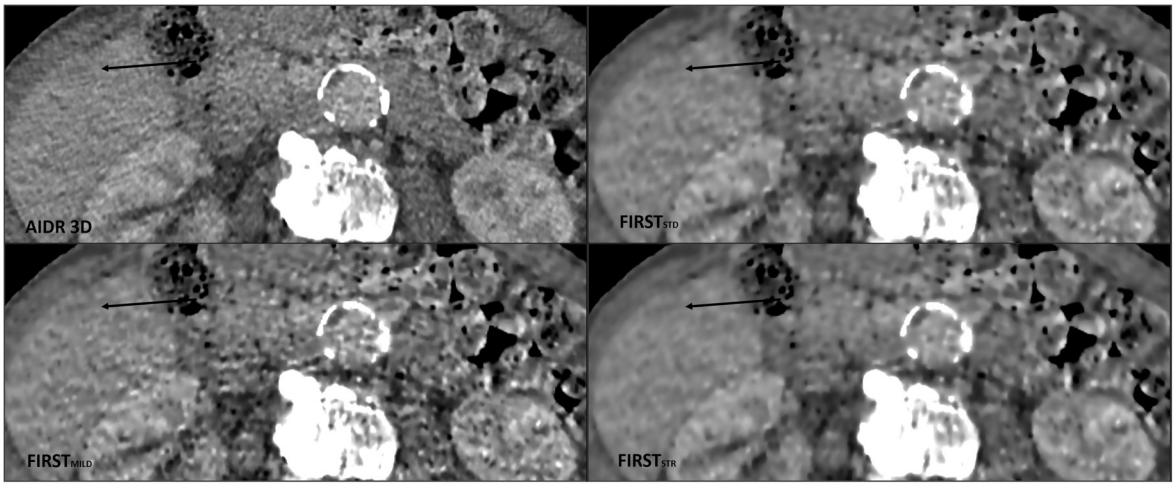

Fig. 3. Axial computed tomography images showing a very low-contrast lesion (black arrows) with liver-to-lesion contrast of 13.60 HU in AIDR-3D, increasing to 16.63 HU in $FIRST_{MILD}$.

showed AIDR-3D not significantly superior. Full results are shown in Table 5.

Evaluation of very low-contrast lesions

With an average lesion signal of 40.47 HU and a SD of 18.70, lesions with a signal of 21.77 HU or less were defined as very low contrast (Fig. 3). Thirteen lesions were included in this group. Average lesion contrast in AIDR-3D reconstruction was 14.12 HU. No significant difference was shown in FIRST reconstructions in this subgroup. SNR and CNR_L showed a significant difference, with $FIRST_{STD}$ and $FIRST_{STR}$ showing improved values and a decrease with $FIRST_{MILD}$. CNR_{BG} was significantly higher with all FIRST reconstructions. Average viewer ratings showed no significant change of any FIRST reconstruction in comparison to AIDR-3D. $FIRST_{STR}$ scored best overall. Full results are shown in Table 6.

Discussion

Our study shows potential in increasing lesion conspicuity with MBIR algorithms. The average lesion signal was increased; in addition, reductions in image noise show substantial increases in CNR with all methods. Of the three different FIRST methods, $FIRST_{MILD}$ shows most promise in lesion analysis, with a 13.3% increase of lesion signal over AIDR-3D. Small lesions, in particular, showed a large signal increase with $FIRST_{MILD}$. Visual analysis of the lesions did not correlate with objective measures, with all FIRST methods being inferior to AIDR-3D and $FIRST_{MILD}$ scoring poorest of all. The reason for this may be a habituation to AIDR-3D images, which are seen by both examiners on a daily basis and have been used at our institution for many years. One examiner noted that FIRST images generally had an "artificial" impression on him.

There has been limited testing of the use of FIRST algorithms in abdominal imaging so far. Tabari et al. showed the possibility of using FIRST reconstruction for sub-Millisievert imaging, showing significant increases in SNR and CNR of abdominal lesions in comparison to FBP in sub-Millisievert CT imaging (27). Our study only evaluated lesions in a standard imaging protocol, without additional analysis of ultra-low-dose imaging. Other applications of FIRST have shown promising results in cardiac CT (28,29) and in the imaging of lung nodes (30,31). Other similar MBIR algorithms have also been tested in liver imaging, showing the ability to further reduce radiation dose while maintaining detectability.

Table 6. Evaluation of very low-contrast lesions.

	AIDR-3D	$FIRST_{STD}$	$FIRST_{MILD}$	$FIRST_{STR}$
Signal (HU) ($P = 1.0$)	14.12	13.72	14.60	13.29
SNR ($P < 0.001$)	4.14 (4.19)	5.78 (5.15)	4.03 (3.88)	6.32 (5.48)
CNR_L ($P = 0.007$)	0.79	1.06	0.75	1.20
CNR_{BG} ($P < 0.001$)	0.48 (0.47)	2.08 (1.53)	2.16 (1.50)	2.00 (1.44)
Viewer rating ($P = 0.795$)	3.42 (3.5)	3.30 (3.0)	3.58 (3.5)	3.23 (3.5)

Values in parentheses are median.
CNR_{BG}, contrast-to-noise ratio with background noise; CNR_L, contrast-to-noise ratio with image noise in liver; SNR, signal-to-noise ratio.

Pickhardt et al. were able to maintain a sensitivity of 79.3% for abdominal lesions with an MBIR algorithm while reducing the dose by an average of 74% (18). Noël et al. showed a significantly better detection with MBIR than with HIR and FBP in 77.9% reduced dose CT images (32). Choi et al. were able to maintain a sensitivity of 97.9% for liver lesions while reducing the dose by one-third with an MBIR algorithm (33).

The present study has some limitations. We retrospectively analyzed lesions that had been noted as poorly contrasted. Due to a large number of radiologists working at our institution, with a wide spectrum of experience in abdominal CT diagnostics, the definition of a poorly contrasted lesion is fairly subjective. This was mitigated by a subgroup analysis of very low contrast lesions. We did not test the impacts of FIRST-LCD on CT scans acquired with imaging protocols designed for lower-dose scanning; therefore, we can only infer from the results of the improved image quality to a potential for dose reduction or better lesion detection. Evaluations of the lesions were only performed in one image slice; as some lesions are inhomogeneous, there may be some slight variations of lesion attenuation in different slices, although the overall small average lesion size may mitigate any effects of this. CNR measurements were performed in reference to image noise in surrounding air, as well as healthy liver tissue. While the improvements in CNR_{BG} were profound with all three FIRST-LCD algorithms, the increases in CNR_L were lower. The measurements of CNR_L may, however, present a more accurate representation of image noise, as air in general should have no attenuation. Multiple lesions in one exam were each classified as singular lesions, omitting a weighting of potential patient specific effects, such as body mass index. Our visual rating only applied to lesion conspicuity; we did not evaluate the subjective image quality of FIRST images as a whole. Based on the improved objective contrast parameters, a prospective head-to-head analysis of AIDR 3D to FIRST-LCD in the sensitivity of liver lesion detection to reference imaging with MRI is warranted to determine true clinical applicability in aiding in the detection of additional lesions.

In conclusion, MBIR algorithms show a promise in increasing image parameters to aid in the detection and characterization of liver lesions. One such algorithm, FIRST-LCD-MILD, was able to significantly improve lesion contrast by >5 HU (+13.27%) and increased the CNR_{BG} by 646.1% in comparison to a hybrid iterative reconstruction method. Our research has also shown improved objective image parameters do not always correlate to a favorable subjective interpretation by radiologists. Subjective scoring of the visual acuity of the liver lesions was poorer in all MBIR methods compared to the original reconstruction, raising the need of further improvements. Further research is required to determine if specialized MBIR algorithms can prospectively lead to improved lesion detection.

Acknowledgements

This study contains results of the thesis "Optimierte modellbasierte Rekonstruktionsverfahren der computertomographischen Bildgebung zur besseren Darstellung von Leberläsionen / Optimized Model-Based Renconstruction Algorithms in Computed Tomography for Better Depiction of Liver Lesions" presented to the Charité – Universitätsmedizin Berlin, corporate member of Freie Universität Berlin, Humboldt-Universität zu Berlin, and Berlin Institute of Health in 2021 by Jonas Oppenheimer.

Keno Kyrill Bressem is grateful for his participation in the BIH Charité Digital Clinician Scientist Program, all funded by the Charité – Universitätsmedizin Berlin and the Berlin Institute of Health.

Declaration of conflicting interests

The author(s) declared the following potential conflicts of interest with respect to the research, authorship, and/or publication of this article: Bernd Hamm has received research grants for the Department of Radiology, Charité – Universitätsmedizin Berlin from the following companies: (1) Abbott, (2) Actelion Pharmaceuticals, (3) Bayer Schering Pharma, (4) Bayer Vital, (5) BRACCO Group, (6) Bristol-Myers Squibb, (7) Charite Research Organisation GmbH, (8) Deutsche Krebshilfe, (9) Dt. Stiftung für Herzforschung, (10) Essex Pharma, (11) EU Programmes, (12) FibrexMedical Inc, (13) Focused Ultrasound Surgery Foundation, (14) Fraunhofer Gesellschaft, (15) Guerbet, (16) INC Research, (17) lnSightec Ud, (18) IPSEN Pharma, (19) Kendlel MorphoSys AG, (20) Lilly GmbH, (21) Lundbeck GmbH, (22) MeVis Medical Solutions AG, (23) Nexus Oncology, (24) Novartis, (25) Parexel Clinical Research Organisation Service, (26) Perceptive, (27) Pfizer GmbH, (28) Philipps, (29) Sanofis-Aventis S.A., (30) Siemens, (31) Spectranetics GmbH, (32) Terumo Medical Corporation, (33) TNS Healthcare GMbH, (34) Toshiba, (35) UCB Pharma, (36) Wyeth Pharma, (37) Zukunftsfond Berlin (TSB), (38) Amgen, (39) AO Foundation, (40) BARD, (41) BBraun, (42) Boehring Ingelheimer, (43) Brainsgate, (44) PPD (Clinical Research Organisation), (45) CELLACT Pharma, (46) Celgene, (47) CeloNova Bio-Sciences, (48) Covance, (49) DC Deviees, Ine. USA, (50) Ganymed, (51) Gilead Sciences, (52) GlaxoSmithKline, (53) ICON (Clinical Research Organisation), (54) Jansen, (55) LUX Bioseienees, (56)

MedPass, (57) Merek, (58) Mologen, (59) Nuvisan, (60) Pluristem, (61) Quintiles, (62) Roehe, (63) SehumaeherGmbH (Sponsoring eines Workshops), (64) Seattle Geneties, (65) Symphogen, (66) TauRx Therapeuties Ud, (67) Accovion, (68) AIO: Arbeitsgemeinschaft Internistische Onkologie, (69) ASR Advanced sleep research, (70) Astellas, (71) Theradex, (72) Galena Biopharma, (73) Chiltern, (74) PRAint, (75) lnspiremd, (76) Medronic, (77) Respicardia, (78) Silena Therapeutics, (79) Spectrum Pharmaceuticals, (80) St Jude, (81) TEVA, (82) Theorem, (83) Abbvie, (84) Aesculap, (85) Biotronik, (86) Inventivhealth, (87) ISATherapeutics, (88) LYSARC, (89) MSD, (90) Novocure, (91) Ockham Oncology, (92) Premier-Research, (93) Psi-cro, (94) Tetec-ag, (95) Winicker-Norimed, (96) Achaogen Inc, (97) ADIR, (98) AstraZenaca AB, (99) Demira Inc, (100) Euroscreen S.A., (101) Galmed Research and Development Ltd, (102) GETNE, (103) Guidant Europe NV, (104) Holaira Inc, (105) Immunomedics Inc, (106) Innate Pharma, (107) Isis Pharmaceuticals Inc, (108) Kantar Health GmbH, (109) MedImmune Inc, (110) Medpace Germany GmbH (CRO), (111) Merrimack Pharmaceuticals Inc, (112) Millenium Pharmaceuticals Inc, (113) Orion Corporation Orion Pharma, (114) Pharmacyclics Inc, (115) PIQUR Therapeutics Ltd, (116) Pulmonx International Sárl, (117) Servier (CRO), (118) SGS Life Science Services (CRO), and (119) Treshold Pharmaceuticals Inc. The funder had no role in the study design, data collection and analysis, decision to publish, or preparation of the manuscript. The remaining authors declare that they have no conflicts of interest and did not receive any funds. There are no patents, products in development, or marketed products to declare.

Funding

The author(s) received no financial support for the research, authorship and/or publication of this article.

ORCID iDs

Jonas Oppenheimer https://orcid.org/0000-0003-3213-0099
Fabian Henry Jürgen Elsholtz https://orcid.org/0000-0001-5258-3250

References

1. Expert Panel on Gastrointestinal ImagingKaur H, Hindman NM, et al. ACR appropriateness criteria® suspected liver metastases. J Am Coll Radiol 2017;14:S314–S325.
2. de Ridder J, de Wilt JH, Simmer F, et al. Incidence and origin of histologically confirmed liver metastases: an explorative case-study of 23,154 patients. Oncotarget 2016;7:55368–55376.
3. Niekel MC, Bipat S, Stoker J. Diagnostic imaging of colorectal liver metastases with CT, MR imaging, FDG PET, and/or FDG PET/CT: a meta-analysis of prospective studies including patients who have not previously undergone treatment. Radiology 2010;257:674–684.
4. Bipat S, van Leeuwen MS, Comans EF, et al. Colorectal liver metastases: CT, MR imaging, and PET for diagnosis–meta-analysis. Radiology 2005;237:123–131.
5. Floriani I, Torri V, Rulli E, et al. Performance of imaging modalities in diagnosis of liver metastases from colorectal cancer: a systematic review and meta-analysis. J Magn Reson Imaging 2010;31:19–31.
6. Schulz A, Viktil E, Godt JC, et al. Diagnostic performance of CT, MRI and PET/CT in patients with suspected colorectal liver metastases: the superiority of MRI. Acta Radiol 2016;57:1040–1048.
7. Krakora GA, Coakley FV, Williams G, et al. Small hypoattenuating hepatic lesions at contrast-enhanced CT: prognostic importance in patients with breast cancer. Radiology 2004;233:667–673.
8. Khalil HI, Patterson SA, Panicek DM. Hepatic lesions deemed too small to characterize at CT: prevalence and importance in women with breast cancer. Radiology 2005;235:872–878.
9. Jones EC, Chezmar JL, Nelson RC, et al. The frequency and significance of small (less than or equal to 15 mm) hepatic lesions detected by CT. AJR Am J Roentgenol 1992;158:535–539.
10. Schwartz LH, Gandras EJ, Colangelo SM, et al. Prevalence and importance of small hepatic lesions found at CT in patients with cancer. Radiology 1999;210:71–74.
11. Solomon J, Marin D, Roy Choudhury K, et al. Effect of radiation dose reduction and reconstruction algorithm on image noise, contrast, resolution, and detectability of subtle hypoattenuating liver lesions at multidetector CT: filtered back projection versus a commercial model-based iterative reconstruction algorithm. Radiology 2017;284:777–787.
12. Singh S, Kalra MK, Hsieh J, et al. Abdominal CT: comparison of adaptive statistical iterative and filtered back projection reconstruction techniques. Radiology 2010;257:373–383.
13. Arapakis I, Efstathopoulos E, Tsitsia V, et al. Using "iDose4" iterative reconstruction algorithm in adults' chest-abdomen-pelvis CT examinations: effect on image quality in relation to patient radiation exposure. Br J Radiol 2014;87:20130613.
14. Mello-Amoedo CD, Martins AN, Tachibana A, et al. Comparison of radiation dose and image quality of abdomino-pelvic CT using iterative (AIDR 3D) and conventional reconstructions. AJR Am J Roentgenol 2018;210:127–133.
15. Geyer LL, Schoepf UJ, Meinel FG, et al. State of the Art: iterative CT reconstruction techniques. Radiology 2015;276:339–357.
16. Mileto A, Guimaraes LS, McCollough CH, et al. State of the Art in abdominal CT: the limits of iterative reconstruction algorithms. Radiology 2019;293:491–503.
17. Thibault JB, Sauer KD, Bouman CA, et al. A three-dimensional statistical approach to improved image quality for multislice helical CT. Med Phys 2007;34:4526–4544.
18. Pickhardt PJ, Lubner MG, Kim DH, et al. Abdominal CT with model-based iterative reconstruction (MBIR): initial results of a prospective trial comparing ultralow-dose with standard-dose imaging. AJR Am J Roentgenol 2012;199:1266–1274.
19. Mileto A, Zamora DA, Alessio AM, et al. CT detectability of small low-contrast hypoattenuating focal lesions: iterative reconstructions versus filtered back projection. Radiology 2018;289:443–454.
20. Millon D, Vlassenbroek A, Van Maanen AG, et al. Low contrast detectability and spatial resolution with model-based iterative reconstructions of MDCT images: a phantom and cadaveric study. Eur Radiol 2017;27:927–937.
21. Hara HMH, Ogawa Y, Chikaraishi K, et al. A new iterative reconstruction CT technique of forward projected model-based IR

solution (FIRST): evaluation of image quality at head CT using a cerebral stroke phantom model. ECR 2019; 2019, Vienna.
22. Hara HMH, Ogawa Y, Chikaraishi K, et al. Low-energy X-ray CT technique in forward projected model-based iterative reconstruction to improve the Low contrast using cerebral stroke phantom model. ECR 2020; 2020, Vienna.
23. Toshiba's AIDR 3D receives FDA clearance. 2012. Available at: https://us.medical.canon/news/press-releases/2012/04/25/1277/ (last accessed 17 October 2019).
24. Irwan RNS, Blum A. AIDR 3D - Reduces Dose and Simultaneously Improves Image Quality (White Paper). Zoetermeer: Toshiba Medical Systems Europe BV, 2011.
25. Toshiba Medical's Fully Integrated Model-Based Iterative CT Reconstruction Receives FDA Clearance. 2016. Available at: https://us.medical.canon/news/press-releases/2016/11/28/2518/ (last accessed 23 October 2019).
26. Joemai RMS, Geleijns J. Forward projected model-based Iterative Reconstruction SoluTion "FIRST" (White Paper). Toshiba Medical Systems Corporation, 2017. Available at: file:///C:/Users/Amreeta/Downloads/CT-WP-Forward-projected-model-based-Iterative-Reconstruction-SoluTion-FIRST.pdf.
27. Tabari A, Ramandeep S, Khera RD, et al. Can fully iterative reconstruction technique enable routine abdominal CT at less than 1 mSv? Eur J Radiol Open 2019;6:225–230.
28. Tatsugami F, Higaki T, Sakane H, et al. Coronary artery stent evaluation with model-based iterative reconstruction at coronary CT angiography. Acad Radiol 2017;24:975–981.
29. Maeda E, Tomizawa N, Kanno S, et al. The feasibility of forward-projected model-based iterative reconstruction SoluTion (FIRST) for coronary 320-row computed tomography angiography: a pilot study. J Cardiovasc Comput Tomogr 2017;11:40–45.
30. Ohno Y, Yaguchi A, Okazaki T, et al. Comparative evaluation of newly developed model-based and commercially available hybrid-type iterative reconstruction methods and filter back projection method in terms of accuracy of computer-aided volumetry (CADv) for low-dose CT protocols in phantom study. Eur J Radiol 2016;85:1375–1382.
31. Fujita M, Higaki T, Awaya Y, et al. Lung cancer screening with ultra-low dose CT using full iterative reconstruction. Jpn J Radiol 2017;35:179–189.
32. Noel PB, Engels S, Kohler T, et al. Evaluation of an iterative model-based CT reconstruction algorithm by intra-patient comparison of standard and ultra-low-dose examinations. Acta Radiol 2018;59:1225–1231.
33. Choi SJ, Park SH, Shim YS, et al. Comparison of image quality and focal lesion detection in abdominopelvic CT: potential dose reduction using advanced modelled iterative reconstruction. Clin Imaging 2020;62:41–48.